

A Massively-Parallel 3D Simulator for Soft and Hybrid Robots

Joel Clay¹, Sofia Wyetzner¹, Alex Gaudio¹, Boxi Xia¹, Andrew Moshova¹, Jacob Austin¹,
Max Segan¹, and Hod Lipson¹

¹Columbia University, New York, NY, United States

Abstract

Simulation is an important step in robotics for creating control policies and testing various physical parameters. Soft robotics is a field that presents unique physical challenges for simulating its subjects due to the nonlinearity of deformable material components along with other innovative, and often complex, physical properties. Because of the computational cost of simulating soft and heterogeneous objects with traditional techniques, rigid robotics simulators are not well suited to simulating soft robots. Thus, many engineers must build their own one-off simulators tailored to their system, or use existing simulators with reduced performance. In order to facilitate the development of this exciting technology, this work presents an interactive-speed, accurate, and versatile simulator for a variety of types of soft robots. Cronos, our open-source 3D simulation engine, parallelizes a mass-spring model for ultra-fast performance on both deformable and rigid objects. Our approach is applicable to a wide array of nonlinear material configurations, including high deformability, volumetric actuation, or heterogeneous stiffness. This versatility provides the ability to mix materials and geometric components freely within a single robot simulation. By exploiting the flexibility and scalability of nonlinear Hookean mass-spring systems, this framework simulates soft and rigid objects via a highly parallel model for near real-time speed. We describe an efficient GPU/CUDA implementation, which we demonstrate to achieve computation of over 1 billion elements per second on consumer-grade GPU cards. Dynamic physical accuracy of the system is validated by comparing results to Euler–Bernoulli beam theory, natural frequency predictions, and empirical data of a soft structure under large deformation.

Introduction

As soft robotics technologies improve and the range of soft materials expands, the ability to interactively model and simulate such systems must keep up [13]. Components of soft robots may be deformable, heterogeneous, self-actuated, or some combination thereof [11]. Traditional finite element physical simulators, while extremely successful at modeling linear physical systems, are challenged by simulating soft non-linear materials efficiently [31] especially when large deformations are involved. The need for adequate simulators for soft robotics is apparent for a variety of reasons, including for design validation, for topology optimization and generative design, and for training controllers in physically-realistic simulation. We propose that mass-spring systems provide a conceptually simple, inexpensive, and accurate solution that can elegantly handle the nonlinearity of highly deformable solids in a manner that is performant for the needs described above. We present the first open-source implementation of a parallelized mass-spring system that both can dynamically operate on upwards of 1 million springs in real time and can enable the simulation of objects with the complex physical properties of smart materials (Fig. 1). Our simulator achieves massive parallelization via a relaxation approach based on techniques developed in the pre-computer era [33].

One facet of soft robotic fabrication that is both challenging and increasingly relevant is the use of multiple interspersed materials within a single component [13]. In order to model a heterogeneous material, the simulator must handle both soft and stiff material within one object. This ability to simulate rigid materials with the same method as deformable materials has generally been bounded by performance. Rigid bodies alone can be simulated with traditional Finite Element Methods efficiently and with high accuracy, but simulations require custom methods for nonlinear elastic materials and actuatable materials. In particular,

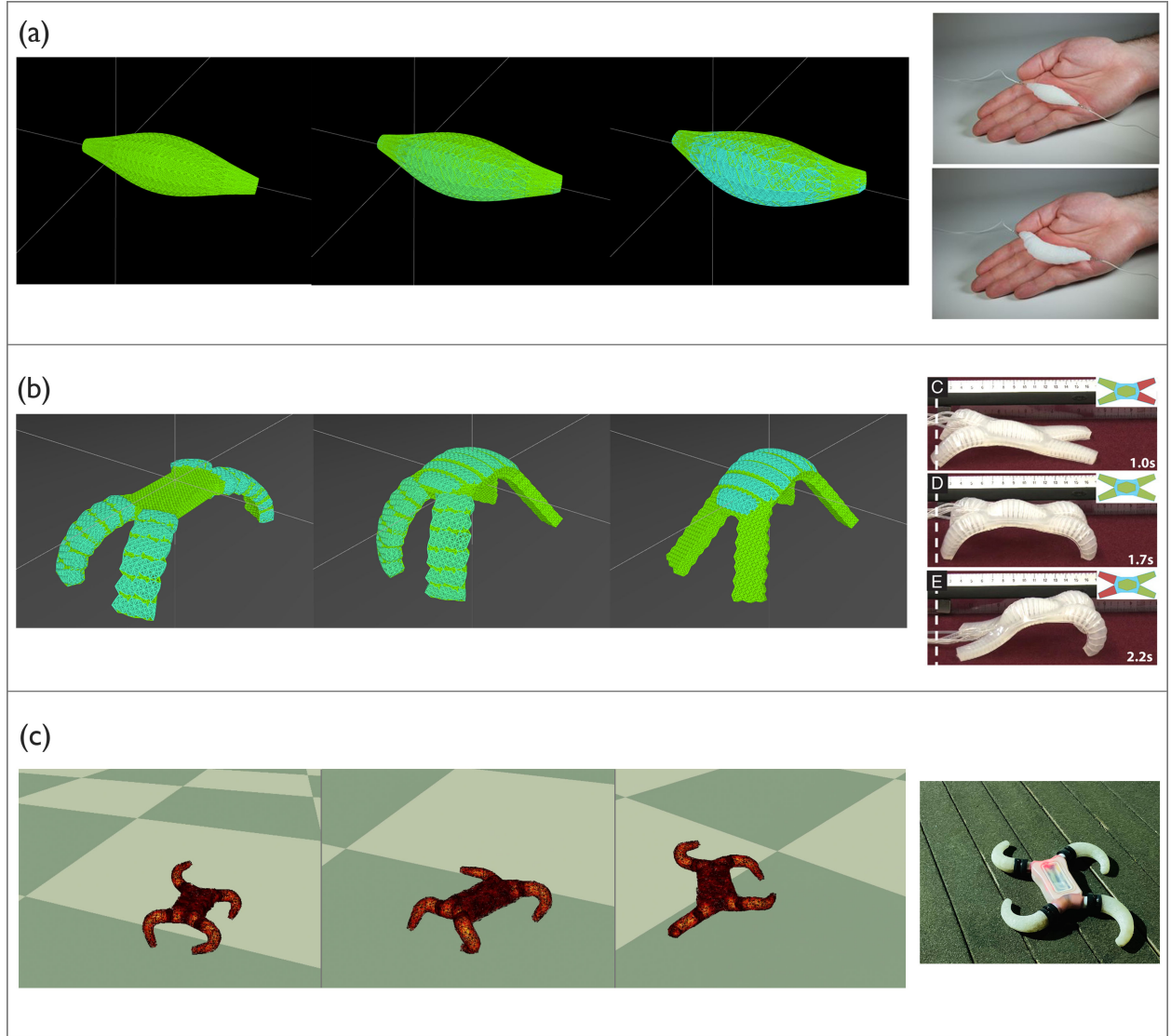


Figure 1: Images on the left contain frames from our method simulating actuation scenarios similar to the real examples on the right. (a) A simulation of the soft thermal actuator from [17] expanding. The actuated portion is slightly offset from the object’s volume to demonstrate a similar pattern to the reference. The reference image on the right is modified from [17]. (b) A simulation of a walking soft robot based off of the seminal pneumatically-actuated soft robot in Shepherd et al.[30]. The simulation is multi-material where actuated material creates periodic joints for limb deformation. The image on the right is modified from [30] (c) A soft robot created by our group simulated by our method. The robot has four soft legs that are actuated by motors attached to their respective rotational joints creating fast locomotion. The simulation captures the resulting deformation and mobility on the left. The image on the right shows the physical robot.

finite element approaches are difficult to parallelize across multiple processors, and therefore do not scale well to massively parallel multicore systems, where most of the price performance gains have been achieved in the past decade [10].

Mass-spring systems are traditionally a simple and fast method for simulating deformable bodies, but become unstable for materials with high Young’s moduli using higher time steps. However, we propose that with a sufficiently small time step, mass-spring systems can handle rigid and deformable components. Optimizing for performance allows us to accommodate materials with very low elasticity in addition to soft materials by using a small time step while also achieving interactive real-time simulation.

Our simulation technique successfully models both rigid and deformable high-resolution objects in interactive real-time. With functional accuracy and subject flexibility, our engine additionally supports high-resolution topologies and interspersed material properties. This opens up possibilities for simulating and fabricating complex soft components quickly, which were previously limited to longer processes. By comparing our simulator to existing systems, we show our simulator’s potential for interactive design and design automation [6] as the first open-source verified-accuracy mass-spring simulation engine.

Deformable/Rigid Body Modeling Methods

There is a large body of work addressing simulation of deformable materials. The computer graphics community has created methods over the past several decades for physics-based visual simulations of soft objects [21]. The ability to use large time steps is valued in computer graphics, as scenes can be complex and need to be rendered in real-time, often without any failure, such as in video game engines. While these motivations are slightly different from the aims of the engineering community, to whom this paper is tailored, the goal of visual accuracy has produced many robust physics-based techniques, which we will discuss here.

There are several high-performant techniques created for graphic simulation of deformable bodies. Liu et al., [14], presents an implicit solver for mass-spring systems that is faster than Newton’s method but not inherently parallelizable. Constraint-based techniques offer a numerically robust alternative to mass-spring models for simulating soft objects. Position Based Dynamics, a popular technique for visually simulating deformations, uses constraint projection on positions rather than force accumulation and integration [20]. Particles update their positions unconstrained, which are then corrected in order to fit elasticity constraints. The method uses a Gauss-Seidel-type solver, and therefore is not easily parallelizable. This method was extended by Bouaziz et al. to incorporate aspects of the Finite Element Method, which improves accuracy and robustness. It uses a Jacobi-type solver for increased (but not full) parallelism [2]. However it has been shown that these methods are not suited to stiff objects or objects with non-constant material properties [36], as they were intended specifically for deformable isotropic solids.

Multi-Materials and Self-Actuation

Few of these methods were created with the intent of simulating multi-material or self-actuated objects. Traditional Finite Element Methods have been shown to become inaccurate for heterogeneous materials, requiring computationally-expensive custom methods to be developed [34]. There has been work on simulating animated characters made of a stiff "skeleton" and a soft surrounding "flesh" using Projective Dynamics [12]. However this technique does not seem to accommodate a spectrum of material stiffness, instead focusing on a rigid-soft binary. Huang et al. presents a numerical simulation method for specifically for actuated soft robotics using second-order integration on a discrete elastic rod model [9]. Their method accurately captures the kinematics of several types of common soft robotics structures, however the method appears to be limited in the realm of larger or multi-material systems. On the other hand, mass-spring models can be implemented with the flexibility to handle a variety of stiffnesses within a single system.

Traditional mass-spring systems have been notably used in graphics to simulate 1D hair [29], 2D cloth [27], and 3D volumetric objects [14]. In non-visual application, mass-spring methods are often used to simulate soft deformable bodies for robotics applications in surgery simulation, due to their suitability for modeling deformations in complex organs composed of different tissue types [16, 23, 37, 5, 15]. Mass-spring systems are capable of handling multiple materials via their inherent discretization of springs. In addition we show that self-actuation can be enabled by dynamically modifying volumetric properties.

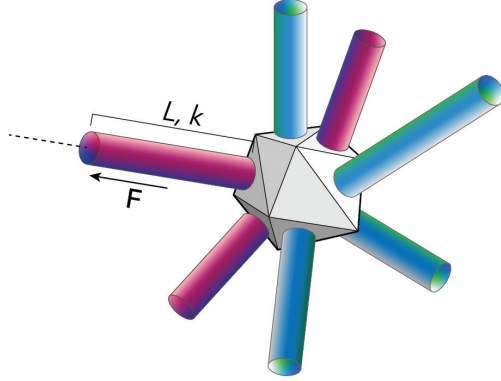


Figure 2: A diagram of a mass and attached springs with irregular geometry. Each spring has a defined rest length, L , and a Hookean spring constant, k , which apply a force, F , to connected masses. Our system allows for minute control over the structural and material properties of the simulated lattice, allowing springs to be individually rigid, actuated, or functionally parameterized.

Simulation Software for Soft Robots

Software packages such as Nvidia PhysX and Nvidia FLeX offer pre-packaged GPU-accelerated implementations of physics-derived graphics algorithms to model physical phenomena [24, 22]. Specifically, both pieces of software rely on a Position Based dynamics approach for deformable bodies [28, 19]. These implementations are either confined to rigid structures or derived from constraint-based physics, therefore limiting their accurate simulation to a smaller range of soft mechanisms.

In soft robotics, there are existing simulation engines intended for simulating physically-accurate components. Our work philosophically builds off of the Voxelyze library [7], which decomposes 3D objects into voxels with discrete material properties, using a mass-spring-like model for simulation. For contrast, our work here does support a voxel-based lattice, but we demonstrate support for more complex geometries as well. Coevoet et al. presents soft robotic simulation software that uses FEM techniques to achieve high physical accuracy for a variety of fabricated soft robots [3]. However these techniques were not specifically designed to achieve real-time performance, especially for more complex discretizations. Hu et al. presents the ChainQueen simulator, a soft-robotics simulation engine that supports many features of novel soft robots, including self-actuation, and heterogeneous materials using the Material-Point Method [8]. The primary focus of ChainQueen is differentiability, which is enabled through our system but not the focal point. Thus there is a space for a fast and usable implementation that can handle a wide array of structures and material properties, for which we provide our solution.

Method

In this section, we review the mass-spring model our implementation utilizes, along with the three integration methods we use for performance and accuracy comparison.

Mass-Spring Force Distribution

Mass-spring systems using Hookean springs distribute forces at each simulation iteration according to Newton’s second law (Fig. 2). These updates can be defined as follows.

The state of each of the N masses in the system is defined by their position $\vec{x}_i(t)$, mass m_i and the total force $\vec{f}_i(t, \vec{x}_i(t))$, $0 \leq i \leq N - 1$. Each mass m_i may be connected to another mass m_j via a spring S_{ij} . (In practice, note that m_i typically has at most C_i spring connections with $C_i \leq 26$.) The acceleration $\vec{a}_i(t) = \frac{d^2 \vec{x}_i(t)}{dt^2}$ of mass m_i is related to the total force \vec{f}_i via Newton’s second law,

$$m_i \vec{a}_i(t) = \vec{f}_i(t, \vec{x}_i(t)), \quad 0 \leq i \leq N - 1. \quad (1)$$

The mass-spring model decomposes \vec{f}_i as the sum of three forces,

$$\vec{f}_i(t, \vec{x}_i(t)) = m_i \vec{g} + \vec{f}_i^{ext}(t) + \sum_{j=1}^{C_i} k_{ij} (|\vec{l}_{ij}(t)| - l_{ij}^0) \frac{\vec{l}_{ij}(t)}{|\vec{l}_{ij}(t)|}, \quad (2)$$

where $m_i \vec{g}$ is the gravitational force, $\vec{f}_i^{ext}(t)$ the external force and the third term is Hooke's Law with $\vec{l}_{ij}(t) = \vec{x}_j(t) - \vec{x}_i(t)$, rest length l_{ij}^0 and spring constant k_{ij} .

The final system to integrate is

$$\frac{d}{dt} \begin{bmatrix} \vec{x}_i(t) \\ \vec{v}_i(t) \end{bmatrix} = \begin{bmatrix} \vec{v}_i(t) \\ \frac{1}{m_i} \vec{f}_i(t, \vec{x}_i(t)) \end{bmatrix}, \quad 0 \leq i \leq N-1, \quad (3)$$

where \vec{v}_i denotes the velocity of m_i , and for given initial position and velocity $\vec{x}_i(0)$ and $\vec{v}_i(0)$.

At this point, a time integration method is used to update positions to the next time iteration.

Time Integration Schemes

Our method uses several explicit time integration schemes in conjunction with the previously-described Hookean force distributions. Explicit time integration methods were chosen over implicit methods for their computational cheapness. The following offers a review of these methods.

We discretize time with a uniform time-step, Δt , and write $t_n = n\Delta t$, $n \geq 0$.

Forward Euler

The formula for this first-order method is for $0 \leq i \leq N-1$,

$$\begin{bmatrix} \vec{x}_i(t_{n+1}) \\ \vec{v}_i(t_{n+1}) \end{bmatrix} = \begin{bmatrix} \vec{x}_i(t_n) \\ \vec{v}_i(t_n) \end{bmatrix} + \Delta t \begin{bmatrix} \vec{v}_i(t_n) \\ \frac{1}{m_i} \vec{f}_i(t_n, \vec{x}_i(t_n)) \end{bmatrix}, \quad n \geq 0. \quad (4)$$

Verlet

Verlet integration is a second-order method that has improved stability and accuracy over forward Euler at no extra performance cost. The formula is given for $0 \leq i \leq N-1$ by

$$\vec{x}_i(t_1) = \vec{x}_i(0) + \Delta t \vec{v}_i(0) + \frac{\Delta t^2}{2m_i} \vec{f}_i(0, \vec{x}_i(0)), \quad (5)$$

$$\vec{x}_i(t_{n+1}) = 2\vec{x}_i(t_n) - \vec{x}_i(t_{n-1}) + \frac{\Delta t^2}{m_i} \vec{f}_i(t_n, \vec{x}_i(t_n)), \quad n \geq 1. \quad (6)$$

RK4

We have also provided an implementation using the fourth order Runge-Kutta method [25]. In practice, we find the algorithm to be stable, but performance suffers drastically since it requires the evaluation at four different stages. Those stages are defined by

$$\vec{a}_i^n = \vec{v}_i(t_n), \quad \vec{A}_i^n = \frac{1}{m_i} \vec{f}_i(t_n, \vec{x}_i(t_n)), \quad (7)$$

$$\vec{b}_i^n = \vec{v}_i(t_n) + \vec{a}_i^n/2, \quad \vec{B}_i^n = \frac{1}{m_i} \vec{f}_i(t_n + \Delta t/2, \vec{x}_i(t_n) + \vec{A}_i^n/2), \quad (8)$$

$$\vec{c}_i^n = \vec{v}_i(t_n) + \vec{b}_i^n/2, \quad \vec{C}_i^n = \frac{1}{m_i} \vec{f}_i(t_n + \Delta t/2, \vec{x}_i(t_n) + \vec{B}_i^n/2), \quad (9)$$

$$\vec{d}_i^n = \vec{v}_i(t_n) + \vec{c}_i^n, \quad \vec{D}_i^n = \frac{1}{m_i} \vec{f}_i(t_n + \Delta t, \vec{x}_i(t_n) + \vec{C}_i^n), \quad (10)$$

and the formula for the update is

$$\begin{bmatrix} \vec{x}_i(t_{n+1}) \\ \vec{v}_i(t_{n+1}) \end{bmatrix} = \begin{bmatrix} \vec{x}_i(t_n) \\ \vec{v}_i(t_n) \end{bmatrix} + \frac{\Delta t}{6} \begin{bmatrix} \vec{a}_i^n + 2\vec{b}_i^n + 2\vec{c}_i^n + \vec{d}_i^n \\ \vec{A}_i^n + 2\vec{B}_i^n + 2\vec{C}_i^n + \vec{D}_i^n \end{bmatrix}. \quad (11)$$

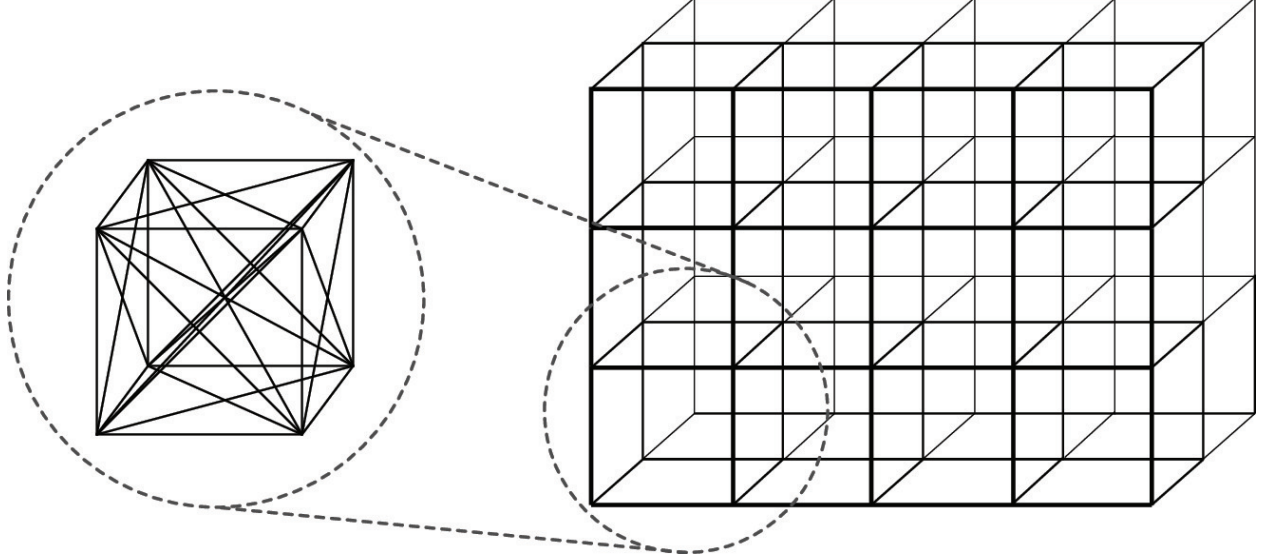


Figure 3: For a voxelized lattice, we build a grid of spring masses by first setting the mass positions, then linking each with neighboring masses to form a cube. We also link the face diagonals (duplicate faces are merged), and long diagonals.

Generating a Lattice

The use of a mass-spring model relies upon discretizing a 3D space into a lattice mesh of nodes and edges (Fig. 4). There are several ways to achieve this, and here we present the two that we used in our testing: (1) Generating a cubic lattice by breaking up the space with a voxel grid; (2) Generating a quasi-uniform lattice via targeted random point selection.

For the former, a voxel grid of desired resolution is overlaid on the object space (most often defined by a 3D mesh file), and nodes which are not inside of the triangle-grid of the object boundaries are culled. Edges are generated between neighboring nodes (Fig. 3). The resolution of this lattice is confined to arrangements describable in voxel form, but the resulting form is straightforward, providing clarity for testing and for multi-material simulations.

For the latter, we aim to sample the 3D space within a bound while maintaining a minimum distance between points. In order to achieve this Poisson disk spacing, we apply a method based on Mitchell’s best candidate algorithm [18]. We begin by placing a single randomly chosen vertex. The following vertex is chosen by generating 100 random candidate vertices, and selecting the vertex which maximizes the distances from its k -nearest neighbors. This is repeated until the desired density of the lattice is achieved. This algorithm yields a quasi-uniform lattice and ensures the vertices are appropriately spaced. We have demonstrated a quasi-uniform mass-spring lattice generated from a 3D mesh of a human femur (Fig. 4).

Once the lattice has been defined, masses are generated from nodes and springs from edges. Physical material properties derive spring constants and mass values. Mass values may be calculated by material density over the tetrahedral volume containing the point mass, or by using a uniform mass distribution based on the total mass of the structure. Spring constants can be derived through material elasticity moduli. Note that a full derivation of spring constants from physical properties is outside of the scope of this paper, but the spring constant often depends the resolution of the lattice in addition to the material elasticity. We have found that a starting point of 0.1 kg per mass with 10,000 as the default spring constant (scaling inversely to the length of the spring) creates a deformable material that can be simulated in real time with a time step of 0.0001. Masses may have external force applied on them, and constraints such as planes might be configured. Finally, the resulting mass-spring lattice is copied to GPU memory to initialize simulation.

GPU Implementation

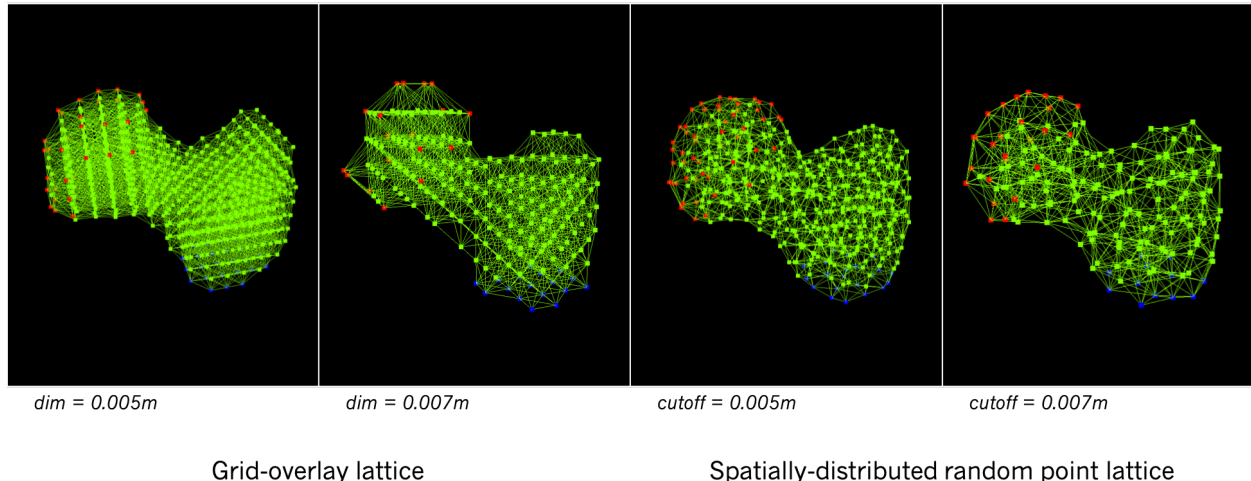


Figure 4: Mass-spring lattices generated from the 3D geometry of a human femur. On the left are two examples of a voxel-based lattice with different resolutions (voxel edge dimension is indicated by "dim"). On the right are two examples of random quasi-uniform lattices generated by a best candidate algorithm with different resolutions (minimum distance is indicated by "cutoff").

The springs and masses are represented internally by classes with member variables to hold necessary state. We store the spring and masses consecutively in memory so that access amongst threads remains fast, and it also allows for faster operations when syncing from CPU to GPU or vice versa.

We duplicate the storage of spring-to-mass connection data since there are cases where using either the GPU or CPU is more suitable for performance. As we store the springs sequentially in memory, the masses can be accessed by iterating through the springs and accessing their endpoints. Our parallel implementation requires that we have the connected springs stored on the mass, so that when visiting each mass, we can iterate through the connected springs and perform the updates accordingly.

Parallel Algorithm

In a naive parallel-update version of the mass-spring system where masses are accessed freely from their connected springs, race conditions arise if the state of a mass is read or written to by multiple threads at once. One way to solve this is by using atomic operations when updating masses. In the typical case of each mass having more than 20 spring connections, these atomic updates can often lead to a situation where threads applying the spring forces will be competing for read/write access on the connected masses.

Depending on the structure of the masses, we have found this to lead to a substantial reduction in throughput. This can be especially problematic with CUDA since the order in which threads are dispatched is undefined, eliminating the strategy of ordering the thread dispatches to minimize duplicate mass updates [26].

We have used a modified algorithm from [19]. The original algorithm solves the race condition by moving atomic operations and adding well-timed thread synchronizations. For double-precision vector operations, we have found that atomic operations lead to reduced throughput due to the need for competing threads to wait on the double-precision operations to complete. In testing, we have found double-precision operations to be up to 10x slower on CUDA than their floating point alternatives.

In order to avoid atomic operations on doubles, the springs are processed first to append their forces to the connected masses. The array of forces on each mass are summed and applied in a later update step. This results in only needing an atomic operation on the integer representing the index to insert into the array. We found this to yield a substantial increase in throughput, allowing our engine to exceed the 1 billion springs /

second barrier.

Algorithm: Parallel Simulation Process

```

forall springs  $S_{ij}$  do
    calculate spring length  $l_{ij} \leftarrow \sqrt{(\vec{x}_j(t) - \vec{x}_i(t))^2}$ 
    calculate spring force  $\vec{f}_{spring} \leftarrow k_{ij}(l_{ij} - l_{ij}^0) \frac{\vec{x}_j(t) - \vec{x}_i(t)}{l_{ij}}$ 
     $m_i \leftarrow masses[i]$ 
     $m_j \leftarrow masses[j]$ 
     $fidx_1 \leftarrow \text{atomicAdd}(m_i.\text{force\_idx}, 1)$ 
     $fidx_2 \leftarrow \text{atomicAdd}(m_j.\text{force\_idx}, 1)$ 
     $m_i.\text{forces}[fidx_1] \leftarrow \vec{f}(spring)$ 
     $m_j.\text{forces}[fidx_2] \leftarrow -\vec{f}(spring)$ 
end
synchronize threads
forall masses  $M_i$  do
    for  $i = 0, i < M_i.\text{force\_idx}, i++$  do
         $M_i.\text{force} \leftarrow M_i.\text{forces}[i]$ 
    end
    // Loop over force_indices and sum into force on mass.
    // Perform position/velocity integration
end

```

Results

In order to validate that the mass-spring system approximates physical systems accurately, we have performed four tests: (1) a Euler–Bernoulli cantilever beam test, (2) a physical accuracy test based on real material behavior, (3) a total energy test to ensure that energy in the system remains constant, and (4) an analytic natural frequency comparison.

Euler–Bernoulli Beam Tests

In order to validate the accuracy of the simulation, standard Euler–Bernoulli beam theory was used to measure the first fundamental frequency of a beam with length L , height H and width W to test against the frequency calculated from the output simulation positions of the same geometry.

The equation for the first fundamental frequency of a horizontal cantilever beam subject to free vibration and a uniformly distributed load (gravity) is,

$$f = \frac{K}{2\pi} \sqrt{\frac{EIg}{\rho AL^4}},$$

where K is a constant corresponding to the first fundamental frequency, E is the modulus of elasticity, $I = H^3W/12$ is the second moment of inertia along the y -axis, g is the gravitational constant, ρ is the mass density, and $A = WH$ is the area of a yz cross-section. Simplifying the formula and treating K , E , ρ , and g as constants yields

$$f \propto \sqrt{\frac{H^2}{L^4}}.$$

Therefore, for varying width, we expect f to be a constant, for varying height, we expect f to be affine, and for varying length, we expect f to decay quadratically.

A small load is applied to the end of the beam to create a deflection. This is on the order of a fraction of a millimeter, because the Euler-Bernoulli theory most accurately predicts small deflections.

The approach is as follows:

1. Apply a small load to the tip of the beam.

2. Begin the simulation with a small amount of simple velocity damping (0.01%).
3. Run the simulation for a set interval (500 ms), until the beam has relaxed.
4. Release the damping and trace the position of the tip over time as the beam vibrates.
5. Determine frequency with a zero-cross count method.

A tip mass of the cantilever beam was chosen in simulation to measure y-position for a period of 1000 simulation milliseconds. The starting y-position of the traced mass is recorded, and the number of times that the mass passes through this point is counted. Once the number of times that the mass crosses through its starting point is determined within a time interval, the frequency of the beam is calculated.

Below, (Fig. 5), we have shown the results of these experiments being run on a variety of beam sizes by independently varying height, width, and length, and calculating the resulting frequency. We compared these with analytical results to determine how closely our mass-spring system follows the Euler–Bernoulli beam theory.

Based on the results, we find that the mass-spring cantilever beam is often a close approximation of what we find in Euler–Bernoulli beam theory. We find that for varying widths, the experimental results are largely greater than the beam theory predicted frequencies. We are not able to determine whether the theory or the experimental results is a better predictor of the physical phenomenon, but the uniqueness of this discrepancy in the Y direction is notable.

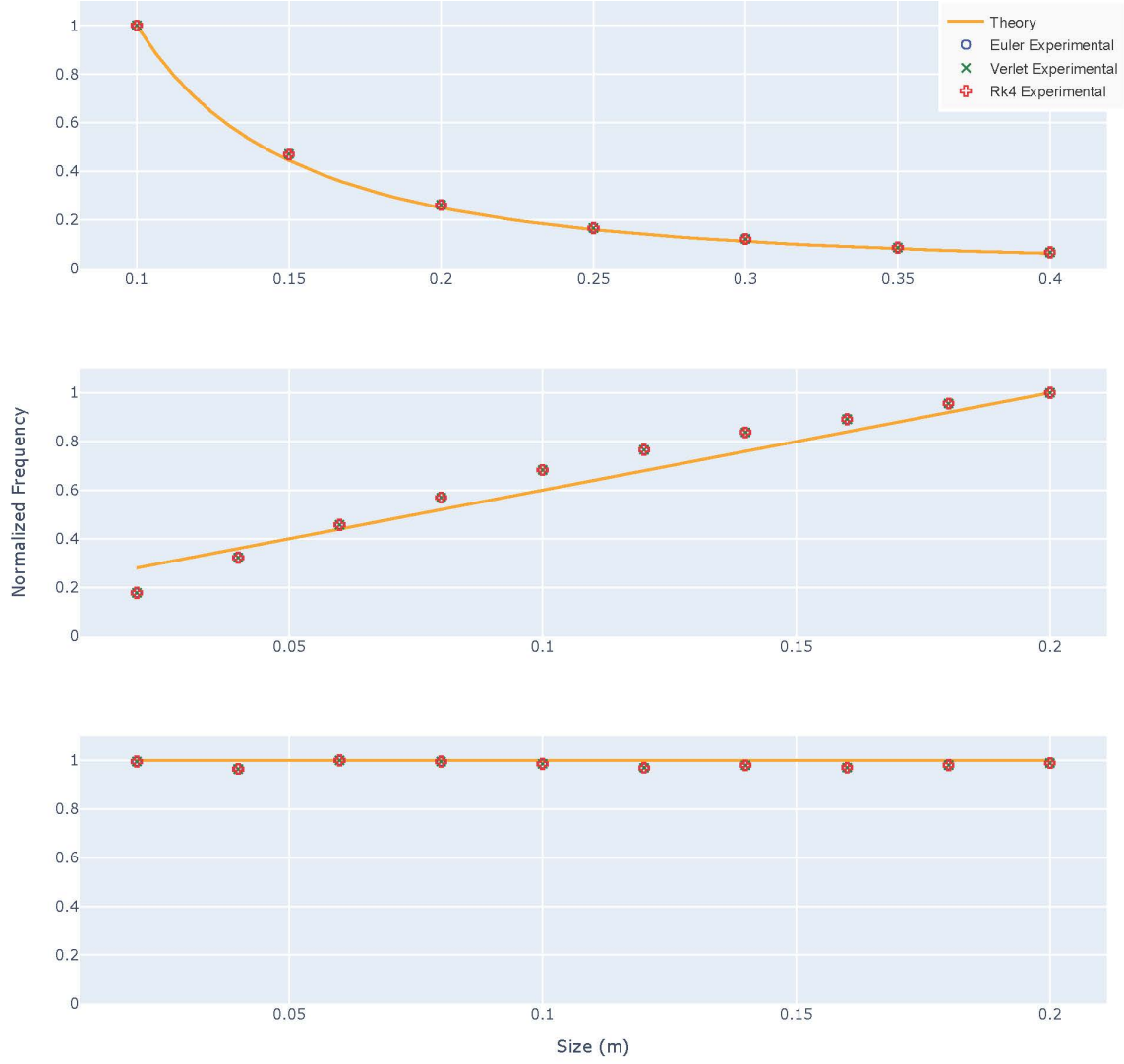


Figure 5: We show normalized frequencies as a function of change in length (top), width (middle) and height (bottom) for the three different timestepping schemes. The output of the normalized frequencies demonstrate that our mass-spring method is a close approximation to expected theoretical values.

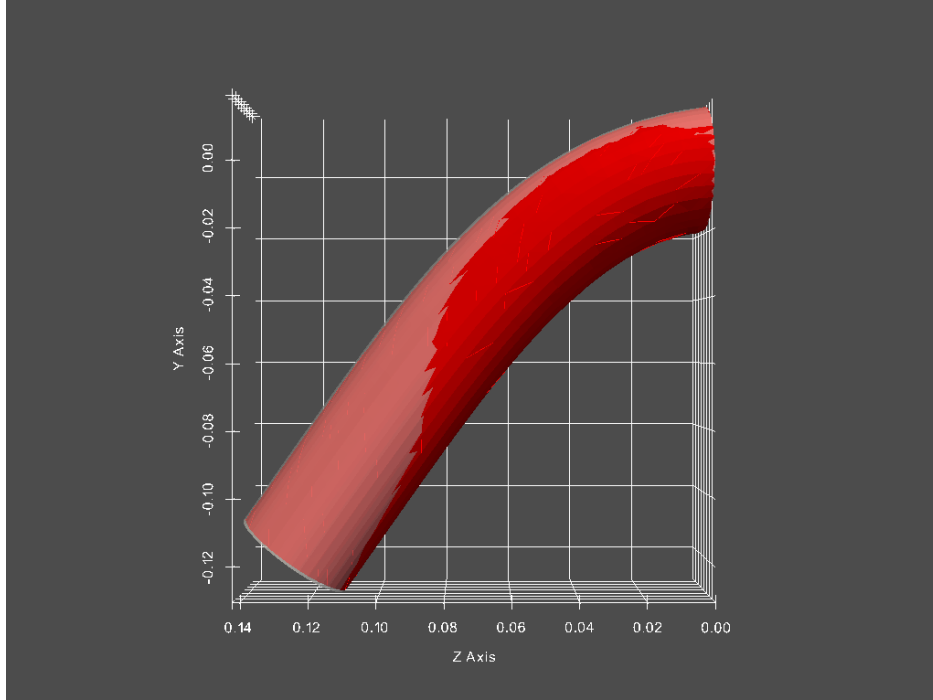


Figure 6: We show accuracy validation of our method for a soft cylinder that has a large deflection applied. The empirical reference is overlaid in white and is from [15]. The result of the deflected cylinder simulated by our method is displayed in red.

Accuracy for Large Deformations

Marchal et al. presents us with an excellent data set for validating large deformations centered around a scan of a physical deformable cylinder along with several traditional simulation methods including three FEM techniques [15]. We have constructed the beam with the parameters described in their paper using our simulation method. The two beams are shown overlapping in Fig. 6. We then perform a surface analysis on the beam relaxed by our method against the empirical beam, whose 3D models can be found as included in the SOFA simulator library [32].

Table 1: We compare our method’s accuracy on large deformations against finite element techniques.

Method	Relative Surface Error (mm)
Mass-Spring [ours]	1.68
Mass-Spring [Marchal et al.]	0.75
Linear FEM Tetrahedral [Marchal et al.]	18.60
Co-rotational FEM Tetrahedral [Marchal et al.]	0.63
Co-rotational FEM Hexahedral [Marchal et al.]	2.87

Table 1 presents a direct comparison between our method and several simulated methods. The empirical beam was used for surface comparison. The co-rotational tetrahedral FEM and listed mass-spring method have less surface error than our method, but the values are comparable. Our method was tuned according to visual accuracy, as in the mass-spring model in Marchal et al. Thus the surface error our method presents could be potentially lower for slightly better parameter values. Our method shows a high level of accuracy, which beats the linear tetrahedral and co-rotational hexahedral FEM surface errors, as tested by Marchal et al. According to the authors’ conclusions, these methods overpredict the deformation significantly.

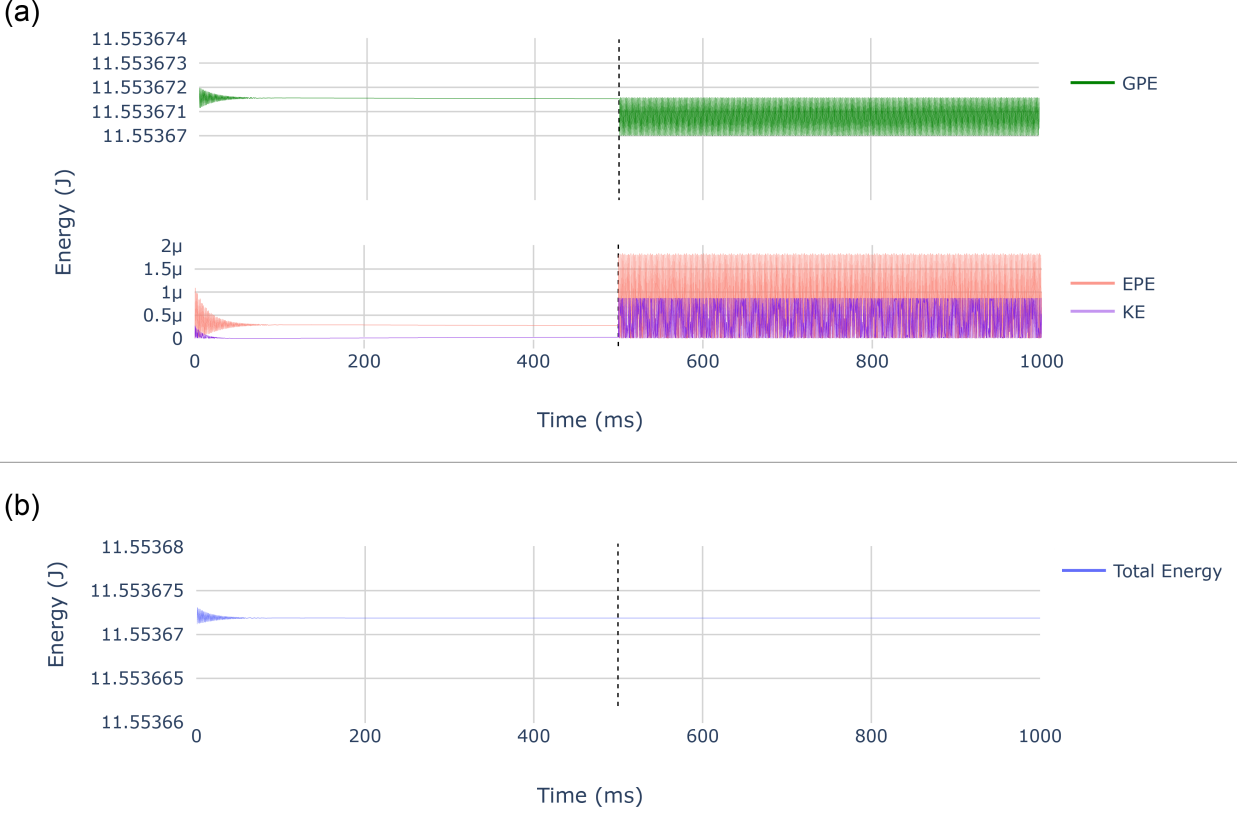


Figure 7: Total energy of the system shows energy conservation after damping is released. (a) demonstrates the components of total energy: EPE = elastic potential energy, GPE = gravitational potential energy, KE = kinetic energy. (b) is a close up view of the total energy sum of (a). The vertical gray lines at 500 ms indicate when the load is released from the beam and damping is set to 0.

Energy Conservation Tests

We have performed energy tests that consist of calculating the elastic potential energy, gravitational potential energy, and kinetic energy of each spring. With this simple validation, we have shown that the mass-spring system obeys the law of conservation of energy. The energy tests were performed in tandem with the beam tests above via the Euler integration scheme.

The results of this test can be seen in (Fig. 7). As expected the system briefly oscillates around an energy value during relaxation while damping is applied, as shown in the beginning of the graphs. In addition, we can see the predicted oscillation of gravitational potential energy, kinetic energy, elastic potential energy during the second half of the test. This indicates the movement of the tip of the beam and resolves to a constant total energy.

Natural Frequency Analysis

To further our validation, we can analytically predict natural frequencies of simulated objects during model runtime. The natural frequency of a system is determined by solving the generalized eigenvalue problem. We construct a mass matrix and a stiffness matrix and then use a sparse Cholesky decomposition solver to calculate the two smallest frequencies. Fig. 8 shows these predicted frequencies in comparison to the actual behavior of the model. Modeled frequency is measured by tracking mass displacement, with the final values calculated via a Fast Fourier Transform. As demonstrated, the behavior of the system closely mirrors the analytical predictions for small deformations. We a discrepancy of 0.56% error for a cantilever beam that has undergone a large deformation, and the resulting graphs have been magnified for clarity. We suspect that

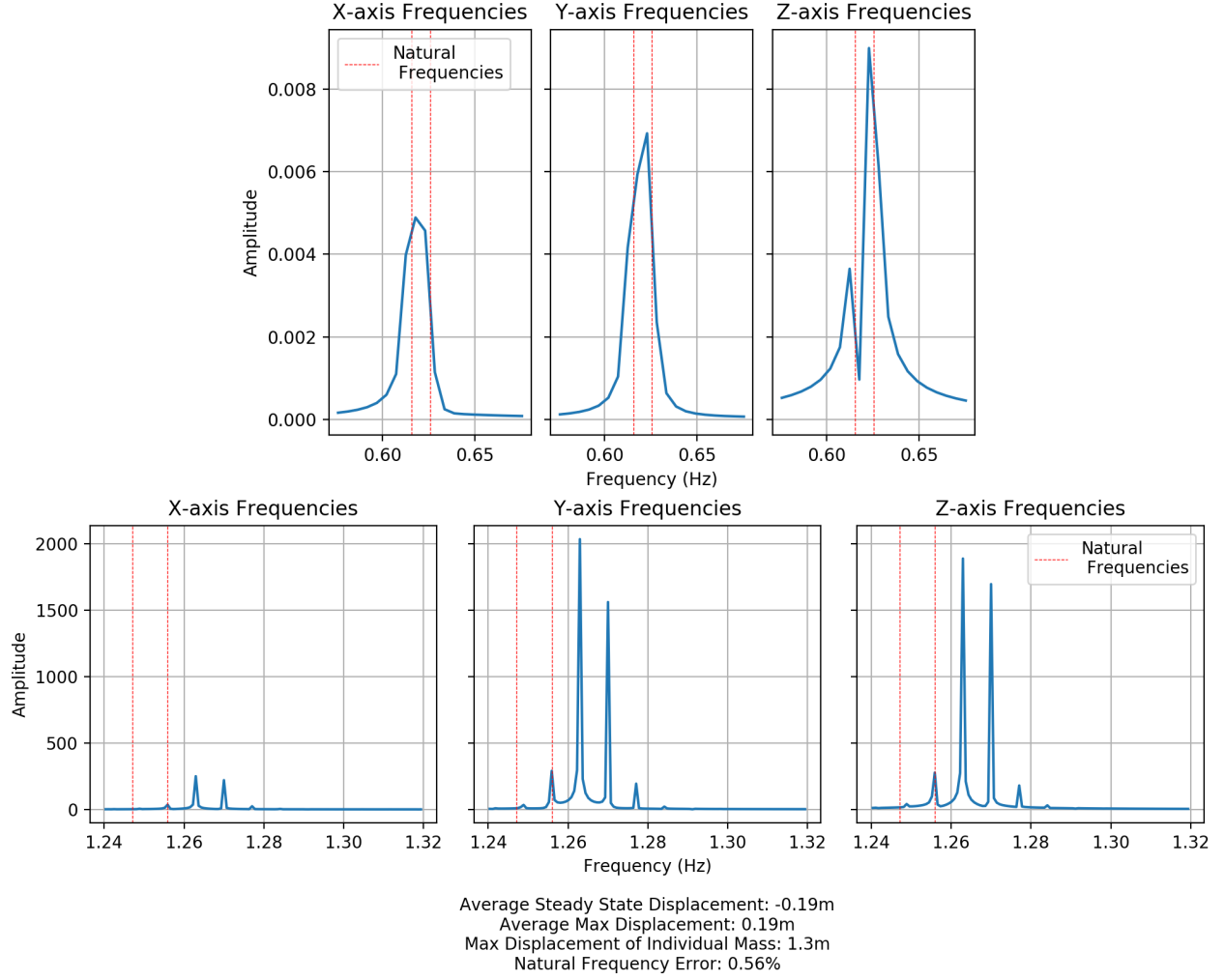


Figure 8: Graphs showing natural frequency prediction on a 10m cantilever beam. The red dotted lines indicate the analytical predictions, with the blue indicating the result of the simulated model under FFT. (Top) Frequency prediction on a cantilever beam under small deformation. As demonstrated, the frequencies are predicted with a high level of accuracy. (Bottom) Frequency prediction on a cantilever beam under large deformation.

this discrepancy is caused by the analytical solution's limits in approximating large deformations, and that the model achieves a behavior closer to reality.

Performance

Below are the results of a performance analysis on our implementation. The analysis was performed on several GPUs and one CPU to demonstrate the speed up due to parallelization. Here, we prove the high efficiency and capacity that this implementation achieves.

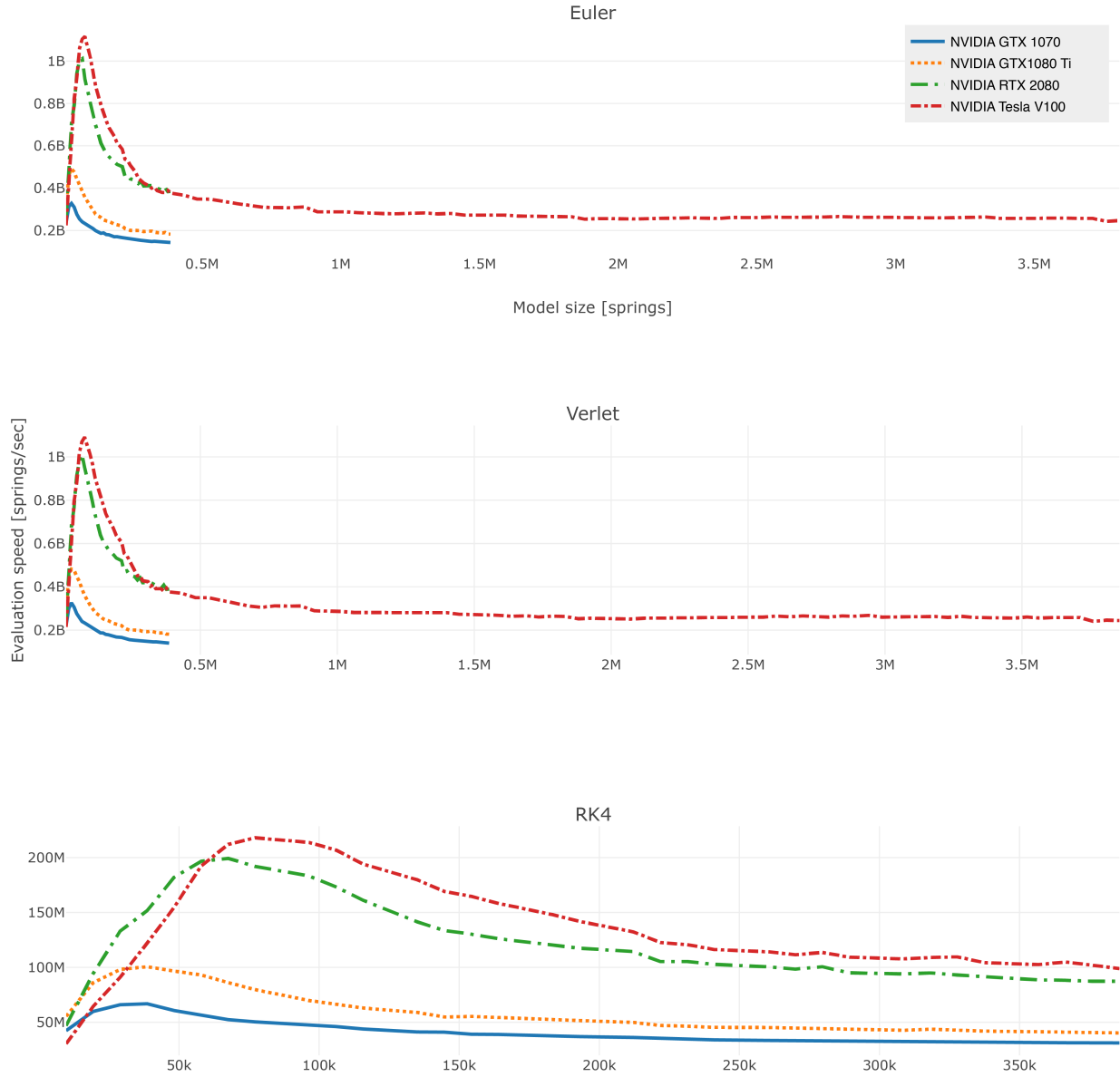


Figure 9: We compare the performance profiles across different integration methods and GPU cards. Euler and Verlet exhibit similar characteristics, while RK4 suffers from dramatically reduced throughput.

Table 3: We compare our performance against other approaches to soft robot simulation software. Note that while the term "particles" accurately describes the discretization technique for both Nvidia Flex and ChainQueen, the best analog in our system are mass elements. "FP" stands for the Forward Propagation operation in ChainQueen as opposed to Backwards Propagation.

Simulator	Particles	Model Iteration Time
Nvidia Flex	8,024	3.5 ms
ChainQueen (FP)	8,000	0.392 ms
Ours	8,000 (active)	0.216 ms

Table 2: We compare the peak performance for an array of computing devices. We achieve over 1B springs per second on Nvidia’s V100 and 2080 RTX, while performance drops significantly for older devices. Further optimizations are possible, as shown in the preliminary results on the RTX 3090.

Device	Bars	Bars/Sec	Cores	Max Clock (GHz)
Nvidia Tesla V100	77.19k	1.12B	5120	1.530
Nvidia RTX 2080	67.55k	1.01B	2944	1.710
Nvidia GTX 1080 Ti	28.99k	492.34M	3584	1.582
Nvidia GTX 1070	28.99k	328.11M	1920	1.683
Intel i7-8700k	9.72k	23.38M	6	4.700
Nvidia RTX 3090 ¹	60.84k	9.11B	10496	1.695

For larger structure sizes, we find that the CUDA implementation yields a nearly 10x improvement in throughput. We notice a performance decrease as the number of masses exceeds the cores on the GPU. This is likely due to the overhead incurred by CUDA’s dispatcher waiting for running threads to finish before dispatching additional threads. If the GPU core count continues growing at the same speed, we predict that the GPU performance will continue to significantly outpace that of the CPU.

In Fig. 9 we demonstrate peak performance on various GPUs. Note that except for the Nvidia Tesla V100, the cards are challenged by loading large model sizes in RAM, and model sizes drop off at around 0.4M springs as a result. We naturally find that peak performance for these GPUs is achieved at far fewer springs than the this limit.

In order to benchmark our simulator against readily available alternatives, we compared performance results based on model iteration time. The data from alternative approaches was replicated from Hu et al [8]. We used a similar test case as the given example with 8,000 active masses and 25 anchored (inactive) masses on the Nvidia GTX 1080 Ti, the GPU used in the Hu et al. benchmarking. Our approach out-performs Nvidia Flex and ChainQueen’s forward propagation (the more similar operation to our step, and also faster than the respective backwards propagation operation in ChainQueen).

Multi-GPU

In these performance tests, we have not considered multi-GPU workstations. Keeping the same level of throughput with Multiple-GPU CUDA support is made difficult by the fact that memory operations must still pass through the PCI-E interface. Due to the way in which the forces propagate throughout the entire structure, we require the changes made on one GPU to be synced to the other GPUs before the next time step. This memory copy operation between GPUs is costly to the throughput as the current PCIe cards can only achieve throughput of up to 32 GB/s. With the recent introduction of NVLink on data center cards, speeds of up to 300 GB/s can be realized [26]. The increase in inter-GPU throughput represents an opportunity to leverage larger GPU core counts. The 10x increase in throughput from NVLink could

¹A further enhancement of the algorithm was used on this device demonstrating further performance improvements, primarily driven by the removal of explicit locking for synchronization.

minimize time waiting for GPU memory copies and enable our parallel implementation to better scale across multiple-GPU configurations.

Applications of the Simulation Method

In Fig. 1 we present several examples of our simulator handling soft robotic components. Visualizations are done through an analogous implementation system of ours, which was built on the same implementation scheme but is slightly slower due to a focus on graphics support [1]. The pneumatically actuated bending robot shown is based on the real-world robot presented in Shepherd et al. [30]. There are five sets of striped actuators, four for each legs and one in the main body, that are activated independently. Notable similar motion is achieved as the physical analog by Sheperd et al.; the motion is shown in our attached supplemental video. In addition the soft-legged locomotive robot developed by our group contains a mix of two materials: a soft material for the legs and a rigid material for the body. We visually tuned material and actuation parameters to achieve likeness to the physical robots in the respective examples. These applications demonstrate our method handling multi-material objects, functional expressions of spring properties, and actuation.

Conclusion

We have introduced the first open-source, massively-parallel, mass-spring simulation engine with verified performance and accuracy. Our implementation of a GPU mass-spring system simulates soft objects with minutely customizable material properties at near real-time speed for interactive simulation and optimization.

Our engine was tested with three different integration schemes for accuracy and performance. On state-of-the-art GPUs our system demonstrates great speed, processing 1 billion spring updates per second. In addition our approach exploits the computational cheapness of mass-spring systems to out-perform alternative soft robotics platforms.

A series of cantilever beam experiments were also run with the software to compare the results to the analytical solutions. In addition we validated our simulator against available physical data of soft materials. We have found the parallel mass-spring method to be a good approximation for simulating deformable and rigid structures.

We have used an interactive GUI on top of this engine to create and modify objects containing over 1 million springs in real time. Figures 1, 4, and supplemental videos were generated via this GUI, which contains the slightly slower version of this method mentioned above that was created for visualization purposes. Our method can also be used to successfully model objects containing multiple materials with varying stiffness and objects with actuated components. Our system is implemented in C++ with the CUDA runtime library and includes Python bindings for further usability. The code is fully open-source, and we hope it will be used to model a wide variety of complex components in soft robotics.

Acknowledgments

This work has been funded in part by U.S. Defense Advanced Research Project Agency (DARPA) TRADES grant number HR0011-17-2-0014 and by Israel Ministry of Defense (IMOD) grant number 4440729085 for Soft Robotics.

An open-source library implementing this simulator is available online [35, 1]. Source code for the software used specifically to perform the experiments described in this paper is available at [4].

Appendix

A. Open Source Library

A fully open source library, Titan, that is actively developed and maintained is available for installation and download at [35]. This library was used for the visualizations of this method, and it uses the OpenGL API to render the results of the engine in real time. Titan was written in C++, but Python bindings are also

available for usability. Titan contains functionality for discretizing soft robots into mass-spring networks and then simulating the bodies with a user-defined time resolution. Constraints may be specified on portions of the robots, which may be directional or planar. Contact planes can be configured to apply frictional forces to robots for simulating locomotion.

References

- [1] Jacob Austin et al. “Titan: A Parallel Asynchronous Library for Multi-Agent and Soft-Body Robotics using NVIDIA CUDA”. In: *arXiv:1911.10274 [cs]* (Nov. 22, 2019). arXiv: 1911.10274. URL: <http://arxiv.org/abs/1911.10274> (visited on 11/26/2019).
- [2] Sofien Bouaziz et al. “Projective dynamics: fusing constraint projections for fast simulation”. In: *ACM Transactions on Graphics (TOG)* 33.4 (2014), p. 154.
- [3] Eulalie Coevoet et al. “Software toolkit for modeling, simulation, and control of soft robots”. In: *Advanced Robotics* 31.22 (2017), pp. 1208–1224.
- [4] *Creative Machines Lab / Cronos*. GitLab. Library Catalog: [gitlab.com](https://gitlab.com/creativemachineslab/OpenDML). URL: <https://gitlab.com/creativemachineslab/OpenDML> (visited on 06/18/2020).
- [5] C. E. Etheredge. “A parallel mass-spring model for soft tissue simulation with haptic rendering in CUDA”. In: *15th Twente Student Conference on IT*. Vol. 15. 2011.
- [6] Jonathan Hiller and Hod Lipson. “Automatic design and manufacture of soft robots”. In: *IEEE Transactions on Robotics* 28.2 (2011), pp. 457–466.
- [7] Jonathan Hiller and Hod Lipson. “Dynamic simulation of soft multimaterial 3d-printed objects”. In: *Soft robotics* 1.1 (2014), pp. 88–101.
- [8] Y. Hu et al. “ChainQueen: A Real-Time Differentiable Physical Simulator for Soft Robotics”. In: *2019 International Conference on Robotics and Automation (ICRA)*. 2019 International Conference on Robotics and Automation (ICRA). May 2019, pp. 6265–6271. DOI: 10.1109/ICRA.2019.8794333.
- [9] Weicheng Huang et al. “Dynamic simulation of articulated soft robots”. In: *Nature Communications* 11.1 (May 6, 2020). Number: 1 Publisher: Nature Publishing Group, p. 2233. ISSN: 2041-1723. DOI: 10.1038/s41467-020-15651-9. URL: <https://www.nature.com/articles/s41467-020-15651-9> (visited on 06/25/2020).
- [10] Stephen W. Keckler et al. “GPUs and the future of parallel computing”. In: *IEEE Micro* 31.5 (2011), pp. 7–17.
- [11] Sangbae Kim, Cecilia Laschi, and Barry Trimmer. “Soft robotics: a bioinspired evolution in robotics”. In: *Trends in biotechnology* 31.5 (2013), pp. 287–294.
- [12] Jing Li, Tiantian Liu, and Ladislav Kavan. “Fast simulation of deformable characters with articulated skeletons in projective dynamics”. In: *Proceedings of the 18th annual ACM SIGGRAPH/Eurographics Symposium on Computer Animation*. ACM, 2019, p. 1.
- [13] Hod Lipson. “Challenges and opportunities for design, simulation, and fabrication of soft robots”. In: *Soft Robotics* 1.1 (2014), pp. 21–27.
- [14] Tiantian Liu et al. “Fast simulation of mass-spring systems”. In: *ACM Transactions on Graphics (TOG)* 32.6 (2013), p. 214.
- [15] Maud Marchal et al. “Towards a Framework for Assessing Deformable Models in Medical Simulation”. In: *Biomedical Simulation*. Ed. by Fernando Bello and P. J. Eddie Edwards. Lecture Notes in Computer Science. Berlin, Heidelberg: Springer, 2008, pp. 176–184. ISBN: 978-3-540-70521-5. DOI: 10.1007/978-3-540-70521-5_19.
- [16] Ullrich Meier et al. “Real-time deformable models for surgery simulation: a survey”. In: *Computer methods and programs in biomedicine* 77.3 (2005), pp. 183–197.
- [17] Aslan Miriyev, Kenneth Stack, and Hod Lipson. “Soft material for soft actuators”. In: *Nature Communications* 8.1 (Sept. 19, 2017), pp. 1–8. ISSN: 2041-1723. DOI: 10.1038/s41467-017-00685-3. URL: <https://www.nature.com/articles/s41467-017-00685-3> (visited on 11/13/2019).
- [18] Don P. Mitchell. “Spectrally optimal sampling for distribution ray tracing”. In: *ACM Siggraph Computer Graphics*. Vol. 25. ACM, 1991, pp. 157–164.
- [19] Damian Mrowca et al. “Flexible neural representation for physics prediction”. In: *Advances in Neural Information Processing Systems*. 2018, pp. 8799–8810.

- [20] Matthias Müller et al. “Position based dynamics”. In: *Journal of Visual Communication and Image Representation* 18.2 (2007), pp. 109–118.
- [21] Andrew Nealen et al. “Physically based deformable models in computer graphics”. In: *Computer graphics forum*. Vol. 25. Wiley Online Library, 2006, pp. 809–836.
- [22] *NVIDIA FleX*. NVIDIA Developer. Aug. 13, 2015. URL: <https://developer.nvidia.com/flex> (visited on 09/05/2019).
- [23] Paolo Patete et al. “A multi-tissue mass-spring model for computer assisted breast surgery”. In: *Medical Engineering & Physics* 35.1 (Jan. 1, 2013), pp. 47–53. ISSN: 1350-4533. DOI: 10.1016/j.medengphy.2012.03.008. URL: <http://www.sciencedirect.com/science/article/pii/S1350453312000562> (visited on 09/05/2019).
- [24] *PhysX SDK*. NVIDIA Developer. Nov. 28, 2018. URL: <https://developer.nvidia.com/physx-sdk> (visited on 09/05/2019).
- [25] William H. Press et al. *Numerical recipes 3rd edition: The art of scientific computing*. Cambridge university press, 2007.
- [26] *Programming Guide :: CUDA Toolkit Documentation*. URL: <https://docs.nvidia.com/cuda/cuda-c-programming-guide/index.html> (visited on 09/05/2019).
- [27] Xavier Provot. “Deformation constraints in a mass-spring model to describe rigid cloth behaviour”. In: *Graphics interface*. Canadian Information Processing Society, 1995, pp. 147–147.
- [28] John Rieffel et al. “Evolving Soft Robotic Locomotion in PhysX”. In: *Proceedings of the 11th Annual Conference Companion on Genetic and Evolutionary Computation Conference: Late Breaking Papers*. GECCO '09. event-place: Montreal, Québec, Canada. New York, NY, USA: ACM, 2009, pp. 2499–2504. ISBN: 978-1-60558-505-5. DOI: 10.1145/1570256.1570351. URL: <http://doi.acm.org/10.1145/1570256.1570351> (visited on 09/20/2019).
- [29] Andrew Selle, Michael Lentine, and Ronald Fedkiw. “A mass spring model for hair simulation”. In: *ACM Transactions on Graphics (TOG)*. Vol. 27. ACM, 2008, p. 64.
- [30] Robert F. Shepherd et al. “Multigait soft robot”. In: *Proceedings of the National Academy of Sciences* 108.51 (Dec. 20, 2011), pp. 20400–20403. ISSN: 0027-8424, 1091-6490. DOI: 10.1073/pnas.1116564108. URL: <https://www.pnas.org/content/108/51/20400> (visited on 10/18/2019).
- [31] Eftychios Sifakis and Jernej Barbic. “FEM Simulation of 3D Deformable Solids: A Practitioner’s Guide to Theory, Discretization and Model Reduction”. In: *ACM SIGGRAPH 2012 Courses*. SIGGRAPH '12. event-place: Los Angeles, California. New York, NY, USA: ACM, 2012, 20:1–20:50. ISBN: 978-1-4503-1678-1. DOI: 10.1145/2343483.2343501. URL: <http://doi.acm.org/10.1145/2343483.2343501> (visited on 09/05/2019).
- [32] *SOFA - Documentation*. SOFA. URL: <https://www.sofa-framework.org/community/doc/> (visited on 03/01/2020).
- [33] R. V. Southwell. *Relaxation Methods in Engineering Science*. Google-Books-ID: mGeUX2ZBVtgC. Oxford, England: Oxford University Press, 1940. 270 pp. ISBN: 978-1-4465-1316-3.
- [34] R. H. W. Ten Thije, Remko Akkerman, and J. Huétink. “Large deformation simulation of anisotropic material using an updated Lagrangian finite element method”. In: *Computer methods in applied mechanics and engineering* 196.33 (2007), pp. 3141–3150.
- [35] *Titan Library*. Creative Machines Lab - Columbia University. URL: <https://www.creativemachineslab.com/titan-library.html> (visited on 10/23/2019).
- [36] Maxime Tournier et al. “Stable constrained dynamics”. In: *ACM Transactions on Graphics (TOG)* 34.4 (2015), p. 132.
- [37] Yu Wang, Shuxiang Guo, and Baofeng Gao. “Vascular elasticity determined mass-spring model for virtual reality simulators”. In: *International Journal of Mechatronics and Automation* 5.1 (2015), pp. 1–10.